AN ORBIT DESIGN METHOD TO SUPPORT SMALL BODY INTERIOR RADAR STUDIES

L. Alberto Cangahuala[(1)], George Minett[(2)]

[(1)] Technical Supervisor, JPL/CalTech, 4800 Oak Grove Drive, Pasadena CA 91109 (USA),E-mail:albe@jpl.nasa.gov
[(2)] Eng. Student, Univ. of Waterloo, Waterloo Ontario N2L EG1 (Canada), E-mail:gminett@engmail.uwaterloo.ca

ABSTRACT

Consider a spacecraft equipped with a radar system that can generate signal returns from both the front and back ends of, as well as any significant voids or composition transitions in, a small body. For the purpose of determining the internal structure and inferring the composition of the body, it is necessary to collect returns from directions that encompass the whole body. Operational constraints include minimization of the survey duration and costs, and an unfamiliarity of the target shape, spin period and direction before arrival.

This paper describes an approach that is robust for a variety of small body shapes and spin directions. The first part of this strategy uses orbits that are stable with respect to solar radiation pressure, at distances where the irregular shape is not a significant consideration. The second part uses orbit orientations that provide coverage at high latitudes not reached in the first part. One forces the eccentricity to evolve from an initial value through zero and back up, typically stretching out the useful time period over a couple of weeks, allowing for safe polar observations. This secular orbit evolution in the second part of the strategy is shown through averaging of the perturbing potential due to the solar radiation pressure force, as well as through numerical simulations. This paper shows orbit selections and coverage metrics for various small bodies, with masses, spin directions and rates that are representative of the observed subset of the total population.

1. INTRODUCTION

There are missions being proposed that would use radio signal reflections to map the interior structure of an asteroid. The orbiting spacecraft would transmit pulses that illuminate the object over various directions and receive echoes reflected from the front and back surfaces as well as interior cracks, voids, and density discontinuities. Synthetic aperture processing and estimation techniques would then be used to form a three-dimensional image of the interior. This technique is referred to as Radio Reflection Tomography (RRT); this proposed application has similar mathematical and physical attributes to medical ultrasonic imaging.

Successful RRT imaging requires having an instrument with sufficient sensitivity to measure reflections from interior composition transitions, and enough power to achieve a reflection off the back surface. For the observation campaign, it is also necessary to (1) collect data from all possible views around the object at sufficiently small spacing between the locations from which the measurements are made and (2) achieve accurate knowledge of the positioning of the radar for each measurement**.**

The mission planning process requires descriptions of the RRT observation campaign. In addition to meeting the above requirements, the campaign should be conducted at a minimum safe distance from the asteroid (so radar power requirements are minimized) and in a minimum amount of time (so operations costs are minimized). Early in the planning, many asteroids (including targets that have not been well-observed from the ground) may be considered. Therefore, the target size, shape, and rotational state used in planning will not be well known, and will vary. However, knowing how much time should be allocated for mapping will help in the overall planning, especially if the mission goals also include sample return and/or visiting multiple asteroids.

A process has been developed by which sensible observation campaigns can be generally defined early in the planning process, followed by more detailed orbit selection. This process addresses the ranges of masses, spin states, and shapes seen in observed Near Earth objects as well as Main Belt Asteroids. In this paper we first describe the RRT observation phase characteristics, as well as the masses and spin rates of likely RRT targets. Second, we describe the dominant small-body effects on mapping orbits, and relevant coverage statistics with examples. Third, we propose a technique that preserves coverage performance in the presence of poor spin directions. Finally, a heuristic analytic technique is developed to provide quick approximations to the calculated coverage durations.

2. RRT OBSERVATION PHASE CHARACTERISTICS

The RRT scenarios that will be considered in this paper will be part of missions with the following characteristics:

- The spacecraft will have single beam radar, using wavelengths on the order of a few tens of meters.
- In order to interpret the radar data collectively, the radial position with respect to the asteroid center of mass will have to be known to a small fraction of the return wavelength (on the order of a meter or less).
- The radar can collect measurements much faster than orbital motion changes the instrument field of view.
- The asteroid is in principal axis rotation.
- The power available for the radar will allow the signal to penetrate through bodies up to approximately 40 km in diameter.
- A chemical propulsive system will be used at the asteroid to place the spacecraft in the mapping orbit(s), and for orbit maintenance.

It is difficult to generate a comprehensive and accurate poll of the masses and spin rates of likely RRT asteroid targets. Nevertheless, it is possible to make some general assessments about the range and distribution of these attributes. 297 asteroids with estimated mean radii < 20 km and estimated rotation periods were selected from [1]. From this sampling, a histogram (see Fig. 1) shows that the majority of estimated rotation periods are less than 10-11 hours. This observation does simplify the orbit selection process, as will be shown in the next section.

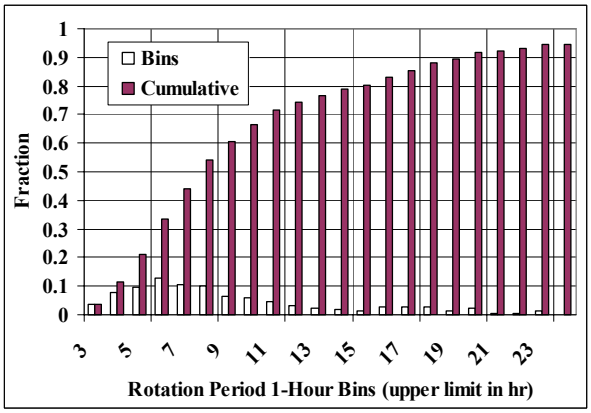

Fig. 1. Rotation Period Histogram (297 asteroid sample)

3. MAPPING ORBITS

Overall, the mapping orbit selection is a tradeoff between the operational simplicity and robustness of a larger orbit versus the speed and lower power requirements of a smaller orbit. In these three-body scenarios, the perturbations due to solar radiation pressure, asteroid oblateness and ellipticity are considered. Solar tide effects dominate at distances much larger than the orbit sizes being considered in this study, so they do not influence orbit selection. Reference [2] describes the perturbations in terms of averaged secular effects on the orbit shape and orientation; the orbit size remains constant on average. These secular effects in general have a characteristic frequency, which can be thought of as the envelope on the rate of change of the relevant orbital elements. The relevant expressions are described in Tables 1-2.

Table 1. Solar Radiation Pressure Orbit Perturbations

Parameter	Averaged Perturbation
de/dt	$-C_g\sqrt{1-e^2}\left[\sin\omega\cos\lambda+\cos\omega\cos i\sin\lambda\right]$
di/dt	$-\frac{C_g e}{\sqrt{1-e^2}}\cos\omega\sin i\sin\lambda$
$d\Omega/dt$	$-\frac{C_g e}{\sqrt{1-e^2}}\sin\omega\sin\lambda$
$d\omega/dt$	$-\frac{C_g\sqrt{1-e^2}}{e}\cos\omega\cos\lambda+\frac{C_g}{e\sqrt{1-e^2}}\sin\omega\cos i\sin$
Characteristic Rate	$C_g=\frac{3G_1}{2BR^2}\sqrt{\frac{a}{\mu}}$

where
(a, e, i, Ω, ω) are the S/C Keplerian Elements,
μ = Asteroid GM, B = S/C mass/area ratio
R = Heliocentric distance G_1 = Solar constant
λ = Ω – N N = Asteroid true anomaly,
and the relevant inertial coordinate frame has the x-axis along the anti-solar direction at epoch and the z-axis normal to the asteroid orbit plane.

Table 2. Asteroid Oblateness Orbit Perturbations

Parameter	Averaged Perturbation
de/dt	0
di/dt	0
$d\Omega/dt$	$-\frac{C_s}{\left(1-e^2\right)^2}\cos i$
$d\omega/dt$	$-\frac{C_s}{\left(1-e^2\right)^2}\left[\frac{5}{2}\sin^2 i-2\right]$
Characteristic Rate	$C_s=\frac{3nJ_2\alpha^2}{2a^2}$

In order to more easily depict some example orbit selections, let's set the target asteroid semi-major axis to 1 AU, the spacecraft area to mass ratio to 40 kg/m^2, the asteroid density to 2.5 g/cm^3, and the spin axis direction to within a few degrees of the asteroid terminator plane (other spin directions are considered in the next section). Fig. 2 shows the effects that define the upper and lower bounds for mapping orbit size for asteroids whose masses range from μ of 10^{-9} to 10^{-3} km^3/s^2 (with the Muses-C target Itokawa noted). As a reference, traces of 3 and 10 mean asteroid radii are included as a function of asteroid mass, as well as the NEAR 35km science orbit around Eros.

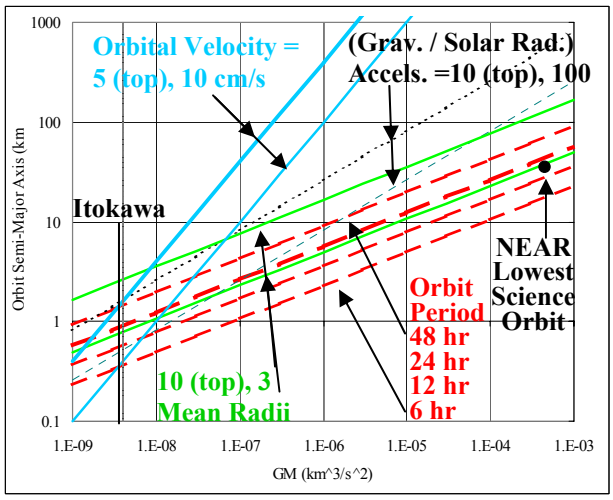

Fig. 2. Mapping Orbit Size Constraints

One upper limit on orbit size, especially for smaller asteroids, is the ratio of gravitational acceleration over solar radiation acceleration. As this ratio drops, the time-averaged orbit plane becomes offset from the asteroid center, and it may not be possible to obtain complete radar coverage of the asteroid. Fig. 2 shows the allowable orbit sizes for a ratio of 10:1. Another upper bound on orbit size for smaller targets is the ability of the propulsive system to properly place the spacecraft into the mapping orbit. The maneuver execution error floor should remain a small fraction (1-2%) of the orbital velocity in order to have a reasonable chance of safely entering and exiting those mapping orbits. Fig. 2 also shows the allowable orbit sizes for mean orbit velocities of 5 and 10 cm/s.

The orbit size lower limit, aside from possible near-field performance limitations of the radar, is due to the irregular shape of the asteroid. The oblateness has no direct secular effect on orbit size or eccentricity; this effect will be revisited in the next section. The ellipticity, however, can lead to instabilities which act on the orbit eccentricity, placing the spacecraft on an escape or crash trajectory. To mitigate this possibility, (1) place the spacecraft in a retrograde orbit, and (2) avoid near-synchronous orbits and orbits resonant with the asteroid's particular elliptical profile. The dashed traces in Fig. 2 show the orbit sizes for a family of orbit periods. Since the majority of asteroid rotation periods are 5-10 hours, setting the lower orbit size limit so that the resulting orbit period is greater than 24 hrs will keep most mapping orbits out of phase with the asteroid shape perturbations. This limit, along with the maneuver execution error limit, make it very difficult, if not impossible, to perform RRT mapping on asteroids with $\mu < 10^{-8}$ km^3/s^2 without a different coverage strategy, such as hovering.

Using the lower size bound, an eccentricity was selected to provide a stable orbit in the terminator plane for a small asteroid. A sample orbit was integrated about an asteroid with a heliocentric distance of ~ 1 AU with $\mu = 3(10^{-8})$ km^3/s^2, shown in Fig. 3. Orbits using an ellipsoid ($J_2 = 0.06$, $C_{22} = 0.01$), and a typical polyhedral gravity field were also generated (not shown) to verify that the solar radiation effects dominated over asteroid oblateness and ellipticity. With the spin direction constrained to the terminator, these orbits are polar and provide more coverage at higher asteroid latitudes than at the equator. However, the terminator orbit provides protection from crashing or escape if the spacecraft were to go into safing during the mapping campaign.

For larger asteroids, the solar radiation pressure effect on the node longitude is dominated by asteroid oblateness, so it is more efficient to use a polar orbit. Fig. 3 shows a sample polar mapping orbit for an asteroid with $\mu = 3(10^{-4})$ km^3/s^2. The asteroid mass range where the two effects are nearly equal (i.e., $C_g = C_s$) is strongly dependent on the heliocentric distance of the asteroid; for Near-Earth Objects with at 24 hr period, the transition is around $\mu = 1(10^{-4})$ km^3/s^2.

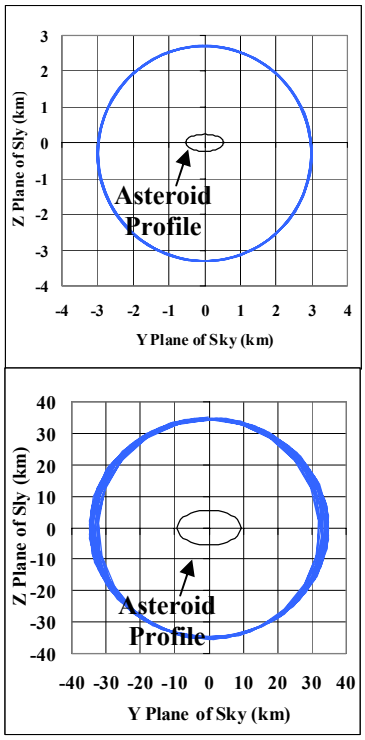

Fig. 3. Asteroid Mapping Orbits ($\mu = 3(10^{-8})$ km^3/s^2 (top), $3(10^{-4})$ km^3/s^2 (bottom))

The relevant RRT coverage metrics are (1) percent coverage of a reference sphere around the asteroid center of mass and (2) the size of the largest continuous unmapped portion of the reference sphere. It is assumed that the objective is to sample evenly across all directions with respect to the center of mass. In practice, there may be features seen upon arrival that would merit augmented coverage (a fissure, sharp changes in surface relief, etc.); the impact of these coverage refinements is left for future analysis.

Coverage is calculated by using evenly spaced points across the reference sphere spaced at particular levels (e.g. 2, 5 deg.). At a time step, the spacecraft position vector is put in dot products against the reference sphere vectors. The point associated with the largest product is the center of the polygon (imagine a soccer ball) that contains the sub-satellite point. Time steps are chosen to ensure that all polygons covered by the spacecraft are identified. The coverage software permits daily outages (say, 2 hr) for data downlink to Earth, as is done in practice. Fig. 4 shows coverage statistics for the two orbit examples. Note that the required coverage duration is independent of asteroid size.

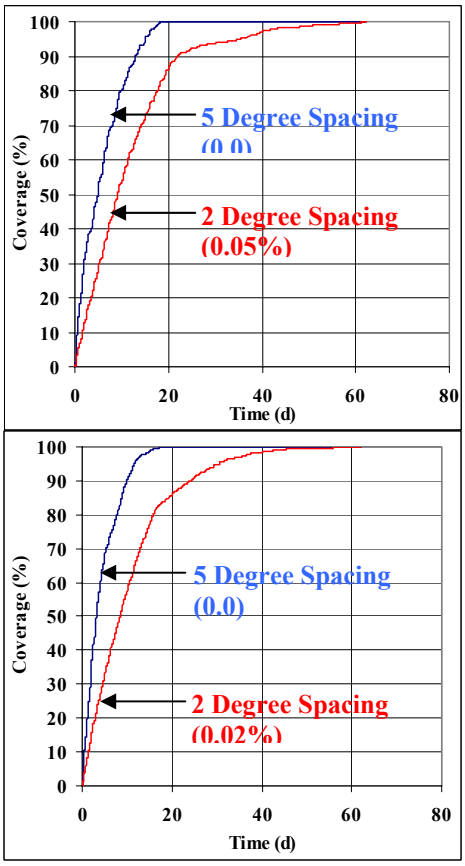

Fig. 4. Coverage ($\mu = 3(10^{-8})$ km^3/s^2 (top), $3(10^{-4})$ km^3/s^2 (bottom), largest uncovered fraction in parentheses)

This algorithm returns the largest uncovered continuous fraction of the reference sphere:

1. Determine all uncovered points and select one.
2. Apply the checks in steps 3-5 to a second point.
3. If the uncovered point is not adjacent to any selected uncovered points, then select the point.
4. If the uncovered point is adjacent to one selected uncovered point, create a list of those points.
5. If the uncovered point is adjacent to multiple selected uncovered points from different lists, add it to the concatenated lists.
6. Repeat Steps 2-5 until all uncovered points have been tested, and select the largest list.

4. NON-TERMINATOR SPIN DIRECTIONS

Up to now, the problem is a bit contrived, as we have limited the spin direction to the terminator plane. If upon arrival, this was not the situation, one option is to wait (and perhaps conduct other investigations) until the terminator plane rotates into alignment with the spin. This may take many months in some cases, and upon closer examination of the perturbation equations, there is an alternative that introduces little risk.

With a non-terminator spin axis, one starts as before, using a terminator orbit to provide coverage at the lower latitudes. Then, one rotates the spacecraft orbit plane about the line of intersection between the original orbit plane and the asteroid orbit plane, resulting in a polar orbit. In this new orbit one forces the eccentricity to evolve from an initial value through zero and back up, typically stretching out the useful time period over a couple of weeks, allowing for safe polar observations. This secular orbit evolution in the second part of the strategy is shown through averaging of the perturbing potential due to the solar radiation pressure force, as well as through numerical simulations. Fig. 5 shows the eccentricity evolution for a polar mapping orbit for an asteroid ($\mu = 3(10^{-8})$ km^3/s^2) with a spin direction at 45 degrees to both the orbit plane and terminator plane. This technique is more effective at larger heliocentric distances and for larger spacecraft mass to area ratios.

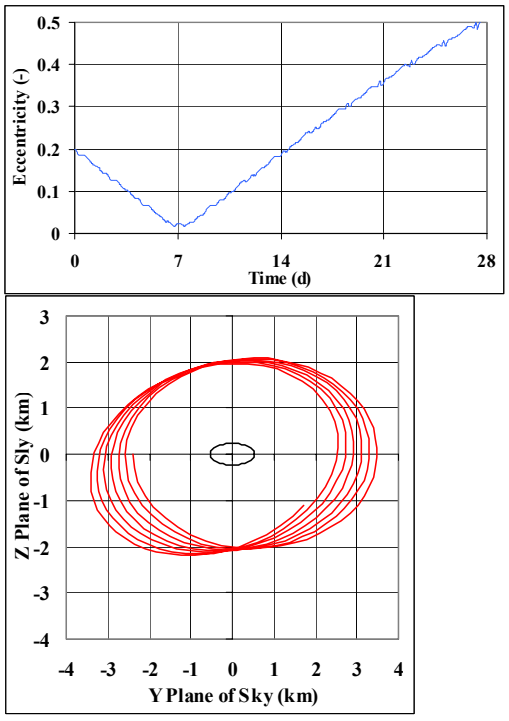

Fig. 5. Eccentricity Evolution for a Polar Mapping Orbit for An Asteroid with a Non-Terminator Spin Direction

Fig. 6 shows the benefit of switching to this eccentric orbit. For the smaller asteroid case shown in Fig. 4, this

orbit is introduced after mapping with the terminator orbit for 20 days (allowing time for the orbit change as well. Essentially complete coverage is obtained in significantly less time for the example shown. Similar benefits can be seen with larger asteroids by adding a retrograde low-latitude orbit to the baseline polar orbit; this additional orbit would require less vigilance than the 'evolving orbit' proposed here.

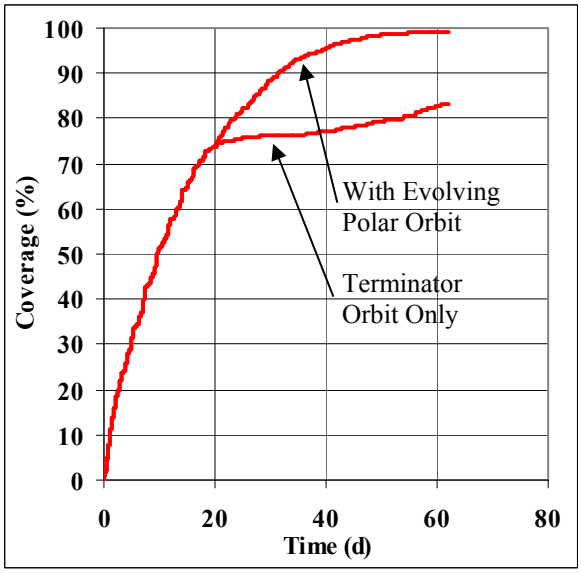

Fig. 6. Coverage Enhancement with the Addition of a Safe Polar Orbit

To conclude this section, and to demonstrate the efficacy of this approach in general, Fig. 7 shows typical orbit radial knowledge using modest amounts of DSN 2-Way X-band Doppler and optical landmark tracking during the mapping campaign. The sub-meter performance is suitable for supporting the RRT reconstruction.

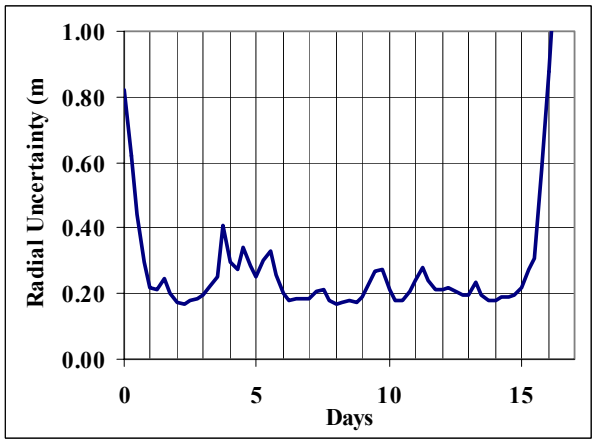

Fig. 7. Orbit Reconstruction Performance (17 d Data Arc, 12 images & 8 hr DSN tracking / day)

5. HEURISTIC ANALYTIC APPROXIMATION

For the mapping orbits and coverage performance levels being considered, it is possible to approximate the duration that a particular orbit is still providing coverage benefits. At each equator crossing, imagine the spacecraft track cutting a swath the width of the desired RRT spacing. Since there is little fine control of the orbit, successive equator crossings can be modelled as essentially random in nature. With a spreadsheet, one can randomly 'drop' swaths at different latitudes until one has obtained complete equatorial coverage; at that time one has essentially obtained complete coverage up to the latitude corresponding to the orbit inclination. The swath width at the equator is shown in Eqn. 1. Fig. 7 shows the effectiveness of these approximations to the results obtained through numerical integration of the trajectory.

$$width = \frac{(C)\sqrt{1+\frac{\omega^2 a^3}{\mu}+2\cos i\frac{\omega a^{3/2}}{\sqrt{\mu}}}}{\sin i} \qquad (1)$$

where C = Coverage Level (deg),

$\omega = 2\pi/(\text{Rotation Period})$.

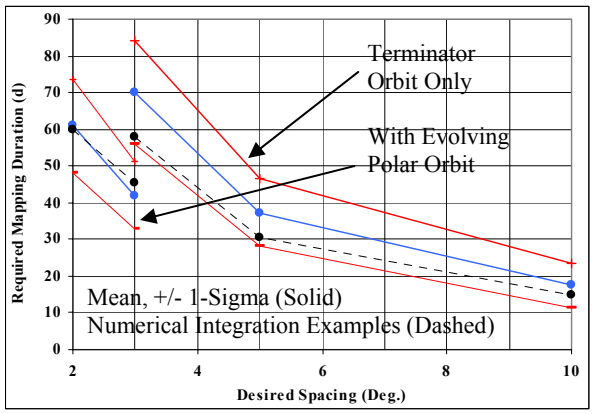

Fig.7. Mapping Duration Approximations ($\mu = 3(10^{-8})$ km^3/s^2, Rotation Period = 6.5 hr)

These approximations are suitable for initial planning purposes.

6. CONCLUSION

From these approximations, the numerical integrations, and the recommended orbit sizing, one can see that the overall RRT mapping duration is more strongly dependent on the spin period and desired coverage level than the asteroid mass and spin direction.

ACKNOWLEDGEMENTS

The work described in this paper was carried out at the Jet Propulsion Laboratory, California Institute of Technology, under a contract with the National Aeronautics and Space Administration. Reference herein to any specific commercial product, process, or service by trade name, trademark, manufacturer, or otherwise, does not constitute or imply its endorsement by the United States Government or the Jet Propulsion Laboratory, California Institute of Technology.

The authors would like to gratefully acknowledge the help and contributions of the following people: Steve Broschart, Ted Drain, Rob Haw, and Ali Safaeinili at the Jet Propulsion Laboratory, and Dan Scheeres at the University of Michigan.

References

1. JPL DASTCOM (Database of ASTeroids and COMets) Database Browser (available to the public at http://ssd.jpl.nasa.gov/dastcom.html).

2. Scheeres, D., "Satellite Dynamics About Asteroids," in Spaceflight Mechanics 1994, Part I, Advances in the Astronautical Sciences Series, Vol 87, pp. 275-292, Univelt, San Diego. Paper AAS 94-112.